

# The structure of binary Lennard-Jones clusters: The effects of atomic size ratio

Jonathan P. K. Doye and Lars Meyer

*Department of Chemistry, University of Cambridge,  
Lensfield Road, Cambridge CB2 1EW, United Kingdom*

(Dated: September 18, 2018)

We introduce a global optimization approach for binary clusters that for a given cluster size is able to directly search for the structure and composition that has the greatest stability. We apply this approach to binary Lennard-Jones clusters, where the strength of the interactions between the two atom types is the same, but where the atoms have different sizes. We map out how the most stable structure depends on the cluster size and the atomic size ratio for clusters with up to 100 atoms and up to 30% difference in atom size. A substantial portion of this parameter space is occupied by structures that are polytetrahedral, both those that are polyicosahedral and those that involve disclination lines. Such structures involve substantial strains for one-component Lennard-Jones clusters, but can be stabilized by the different-sized atoms in the binary clusters. These structures often have a ‘core-shell’ geometry, where the larger atoms are on the surface, and the smaller atoms are in the core.

PACS numbers: 61.46.+w,36.40.Mr

## I. INTRODUCTION

There has been much recent interest in binary clusters, both from a fundamental and a technological perspective. For example, alloy clusters are of particular importance, because of their potential catalytic properties.<sup>1,2</sup> Furthermore, binary clusters offer the opportunity to tailor their properties through the choice of atom types and composition, potentially leading to new behaviour that is not possible for single component clusters. Here our focus is on the structure of binary clusters, which is one of their most important properties, and is a prerequisite for understanding many of the other properties of such clusters.

For monoatomic clusters, Lennard-Jones (LJ) clusters provide a well-characterized model system, for which the effects of a cluster’s finite size on the structure, thermodynamic and dynamic properties are well understood. For example, putative global minima are now available for all LJ clusters with up to 1600 atoms,<sup>3,4,5,6,7,8</sup> and the size evolution of the structure of larger clusters is well understood.<sup>9,10,11</sup>

For binary clusters, there is a similar need for an archetypal system to understand the effects that can control the structure of a binary cluster. We propose that binary Lennard-Jones (BLJ) clusters could provide just such a model system, and this paper aims to start the systematic exploration of this model. One advantage of using BLJ clusters as a model system is the relative simplicity of the potential. There are only four effective parameters that characterize the interactions between the different combinations of atoms, making it possible to systematically study the structure of BLJ clusters as a function of these parameters. By contrast, even the simplest many-body metal potential would have a considerably greater number of parameters, and so it only becomes feasible to study a series of example binary metal systems, which just represent a set of points in this state space of potentials.

Binary clusters also offer considerable additional challenges to the theoretician, compared to the one-component case. Firstly, for a given cluster, there are many more minima on the potential energy surface, because of the presence of “homotops”,<sup>12</sup> isomers with the same geometric structure, but which differ in the labelling of the atoms. Secondly, the composition provides an additional variable to consider. For example, the task of obtaining the lowest-energy structures for all compositions and all sizes up to 100 atoms would require 5050 different global minima to be found. Instead, most studies have either just considered a few sizes and explored how the structure depends on composition,<sup>13,14,15,16,17</sup> or kept the composition fixed and studied the size dependence.<sup>18,19</sup> By doing such a selective survey, there is the possibility that the most interesting and stable structures for the systems are missed.

Here, we take a different approach, neither trying to find the global minima for every size and composition, nor taking an arbitrary cut through this space. Since one is usually just interested in particularly stable structures, finding all the global minima is unnecessary, and so we instead directly search for these particularly stable structures. In particular, we use the composition as a variable in our global optimization and for a given size we attempt to find the most stable composition.

Our focus in this paper is to use BLJ clusters to understand how different types of cluster structure can be stabilized purely through the two atom types being of different size. In particular, we are interested in polytetrahedral structures,<sup>20</sup> for which all the occupied space can be divided up into tetrahedra with atoms at their corners. For a one-component system such packings are said to be ‘frustrated’, because regular tetrahedra do not tessellate, as illustrated in Fig. 1. The best local packing of tetrahedra involves packing five tetrahedra around a common edge, but with regular tetrahedra there is a small angular deficit. As larger structures are made up

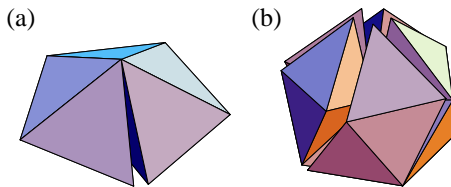


FIG. 1: (Colour online) Examples of the strain involved in packing tetrahedra. (a) Five regular tetrahedra around a common edge produce a gap of  $7.36^\circ$ . (b) Twenty regular tetrahedra about a common vertex produce gaps equivalent to a solid angle of 1.54 steradians.

of regular tetrahedra, these gaps grow rapidly in size. So for a 13-atom icosahedron, which can be thought of as a packing of 20 slightly irregular tetrahedra around a common vertex, the distance between adjacent atoms on the surface is 5.15% longer than that between the central atom and a surface atom. For monoatomic systems, there will be an energetic penalty associated with this strain. However, the associated strain can be completely removed in a binary system simply by choosing the central atom to be 9.79% smaller. Similarly, Frank-Kasper phases, bulk polytetrahedral crystals, are only found for alloys.<sup>21,22,23</sup> Furthermore, stabilization of polytetrahedral structures in binary metal clusters in which there is a size mismatch between the two atom types has previously been seen.<sup>13,14,15</sup>

In section II we describe the choice of potential parameters, how we analyse the energetics, and our global optimization approach. In section III A, for three cluster sizes we present case studies of how the lowest-energy structures depend on both the composition and the atomic size ratio, and in section III B we present our systematic survey of the optimal structures and compositions for all clusters with up to 100 atoms and up to 30% difference in atom size. A brief report of some of the work presented here has appeared previously.<sup>24</sup>

## II. METHODS

### A. Potential

Here, we use a binary Lennard-Jones (BLJ) potential:

$$E = 4 \sum_{i < j} \epsilon_{\alpha\beta} \left[ \left( \frac{\sigma_{\alpha\beta}}{r_{ij}} \right)^{12} - \left( \frac{\sigma_{\alpha\beta}}{r_{ij}} \right)^6 \right], \quad (1)$$

where  $\alpha$  and  $\beta$  are the atom types of atoms  $i$  and  $j$ , and  $\epsilon_{\alpha\beta}$  and  $2^{1/6}\sigma_{\alpha\beta}$  are the pair well depth and equilibrium pair separation, respectively, for the interaction between atoms  $i$  and  $j$ . In its most general form the BLJ potential has four effective parameters, namely  $\epsilon_{AB}$ ,  $\epsilon_{BB}$ ,  $\sigma_{AB}$  and  $\sigma_{BB}$ , if  $\epsilon_{AA}$  and  $\sigma_{AA}$  are used as the units of energy and length, respectively. Here, as we wish to

consider the effects of purely the size ratio on the most stable structures, we choose  $\epsilon_{AA} = \epsilon_{AB} = \epsilon_{BB} = \epsilon$ . Furthermore, as we define  $\sigma_{AB}$  using the Lorentz rule,  $\sigma_{AB} = (\sigma_{AA} + \sigma_{BB})/2$ , in this case there is effectively just one parameter in the potential, namely the size ratio of the two atoms,  $\sigma_{BB}/\sigma_{AA}$ .

Initially, we thought of directly searching for the most stable composition and size ratio for a cluster of a particular size in our global optimization runs. However, we quickly found that increasing the size disparity between the two types of particles leads to a virtual monotonic decrease in the energy. Consequently, our optimization runs led to structures with huge differences in the sizes of the atoms. These structures consist of a core of tiny atoms surrounded by a shell of large atoms, where the large atoms are able to interact strongly with all the atoms in core. They are clearly unphysical and so this approach was abandoned in favour of using only the composition as a variable during the global optimization, and considering different size ratios independently.

We chose to look at the structures for size ratios in the range  $1 < \sigma_{BB}/\sigma_{AA} < 1.3$ , as we wished to see if polytetrahedral structures would be stabilized as we move away from the one-component Lennard-Jones reference system (i.e.  $\sigma_{BB}/\sigma_{AA} = 1$ ). Due to the symmetry of the energetic interactions, exactly the same structural behaviour will be seen in the parameter range  $0.769 < \sigma_{BB}/\sigma_{AA} < 1$ , except that the role of the A and B atoms will be reversed. Six values were considered; namely,  $\sigma_{BB}/\sigma_{AA} = 1.05, 1.1, 1.15, 1.2, 1.25$  and  $1.3$ .

There has been a certain amount of previous work on binary LJ clusters, as a general model for binary systems,<sup>25,26,27,28,29</sup> as a model of binary rare-gas clusters<sup>16,30,31,32,33</sup> and as a playground for testing how the potential parameters could be used to tailor the cluster's structural properties.<sup>32,34,35,36</sup> Of these studies, a few have considered the same set of parameters as we have here,<sup>25,27,29</sup> with some tendencies to form core-shell clusters noted.<sup>25,27</sup> However, nothing like the systematic survey presented here has been tried previously.

To apply the current approach, one needs to be able to compare the relative stabilities of clusters with the same number of atoms but different compositions. For the current system, as all the  $\epsilon_{ij}$  are the same, the most natural way is to compare their absolute energies directly.

For systems, where the energetic interactions are more varied, this issue becomes more subtle. There are a number of approaches one might take depending on to what the 'stability' is being measured with respect. For example, a simple approach would be to compare the energies to a linear interpolation between the energies of the pure systems. In bulk, this would amount to comparing the stability with respect to separation into the pure phases. For clusters, it would be sensible to somewhat amend this approach, as it would automatically put the pure clusters on the same energetic footing, irrespective of whether they represented particularly stable sizes (or not) for the pure systems. For instance, one could in-

stead measure the energies with respect to a linear interpolation between smoothly varying functions, call them  $E_{\text{ave}}^\alpha(N)$ , that captured the general size dependence of the energies of the pure clusters.

Alternatively, one might be interested in maximizing the stability of the cluster with respect to the liquid state, i.e. finding the composition with the maximum melting point. For example, for systems where the cross-terms favour mixing, there will be a stabilization of intermediate compositions for both the solid and the liquid, and so a non-linear interpolation would be required to detect enhanced thermostability from the background mixing effects.

In order to understand better how particular structures are stabilized, it is useful to decompose the energy into different terms. Firstly, we divide the energies into contributions from those pairs of atoms that are nearest neighbours from those that are not, i.e.

$$E = E_{\text{nn}} + E_{\text{nnn}} \quad (2)$$

where  $E_{\text{nn}}$  and  $E_{\text{nnn}}$  are the energetic contributions from nearest neighbours and non-nearest neighbours. Nearest neighbours are simply defined using a distance criterion. In practice we used 1.3 times the relevant equilibrium pair separation, but as there is usually a clear separation between nearest-neighbour and next-neighbour shells for the ordered structures that we find to be the global minima, the precise value is not critical.

Secondly, we divide up  $E_{\text{nn}}$  by defining a strain energy in terms of the difference in energy between the nearest-neighbour energy, and the energy this term would have if all the nearest neighbours had the same separation (measured with respect to the relevant equilibrium pair separation): i.e.

$$E_{\text{nn}} = n_{\text{nn}} V_{LJ}(r'_{\text{nn}} \sigma) + E_{\text{strain}}, \quad (3)$$

where  $n_{\text{nn}}$  is the number of nearest neighbours, and  $r'_{\text{nn}}$ , the reduced average separation of these nearest neighbours is defined as  $\langle r_{ij} / \sigma_{\alpha\beta} \rangle_{\text{nn}}$ , where the average is taken over only those pairs of atoms that are nearest neighbours.<sup>37</sup> Hence,  $E_{\text{strain}}$  measures the energetic penalty arising because a structure has a distribution of nearest-neighbour distances.

As  $E_{\text{nnn}}$  is relatively insensitive to structure, the best structure is determined mainly by the balance between maximizing  $n_{\text{nn}}$  and minimizing  $E_{\text{strain}}$ . For one-component polytetrahedral clusters, both  $n_{\text{nn}}$  and  $E_{\text{strain}}$  are usually large, and by following  $E_{\text{strain}}$  as a function of  $\sigma_{BB}/\sigma_{AA}$  will allow us to see how this strain can be relieved by having different sized atoms.

## B. Global optimization

The basin-hopping global optimization algorithm<sup>4,38</sup> has proved to be very successful for the optimization of a wide range of clusters. The method simply involves

doing a constant temperature Metropolis Monte Carlo simulation, where after each step a local minimization is performed on the resulting configuration, and the acceptance criterion is based upon the energies of these minimized configurations. The success of the method is because it effectively searches a transformed potential energy surface, for which the dynamics and thermodynamics is more helpful for optimization.<sup>39,40</sup>

In addition to the standard basin-hopping moves (random displacements of all atoms and rotations of low-energy atoms around the centre of mass) used for one-component systems, for binary clusters it is important to incorporate moves into the algorithm that allow efficient exploration of the space of homotops and composition. The two moves that we used involved swapping the identities of an A and a B atom,<sup>16</sup> and changing the identity of a single atom. In optimizations runs where the composition was held fixed, only the former composition-preserving moves were used. Typically, these types of moves represented 50% or more of the total moves.

The current optimization task of finding the structure and composition of a binary cluster that has the lowest energy (we shall call this the ‘compositional global minimum’) is very challenging, because the number of possible structures increases very rapidly with size. Firstly, the number of geometric isomers scale as  $\exp(\alpha N)$ .<sup>41,42</sup> Secondly, the number of possible homotops for a given geometric structure is proportional to  $\binom{N}{N_A}$  (assuming that all the homotops are locally stable). Thirdly, the number of possible compositions increases linearly with  $N$ . For example, for LJ<sub>100</sub> the estimated number of geometric isomers is of the order of  $10^{39}$ . If all these are stable for the binary clusters and all homotops are possible, this then gives an estimate of  $10^{69}$  energetically different minima in the space that we search to find the compositional global minimum of BLJ<sub>100</sub>. It is, therefore, important that we make as much use of the structural information gleaned from unbiased runs to aid the optimization task.

Our initial strategy was to perform an initial series of runs for each cluster size from random starting points at a moderate temperature, similar to that typically used for one-component LJ clusters. Subsequently, we performed low temperature runs from the best structures found from the above runs. The rationale is that for  $\sigma_{BB}/\sigma_{AA}$  values sufficiently close to one, the energy differences between homotops can be significantly smaller than that between geometric structures. For example, this feature manifests itself in the thermodynamics of such binary clusters as low-temperature heat capacity peaks associated with permutational disordering.<sup>33,43</sup> The hope is then that the high temperature runs would find the best geometric structures, and the low temperature run the best homotop consistent with this geometric structure. At larger  $\sigma_{BB}/\sigma_{AA}$ , this separation of energy scales breaks down, and so the low-temperature runs are less important. We also performed series of runs, where the best structure for a particular size and size ratio were used as starting points for basin-hopping runs at different size ra-

tios and sizes (with the requisite number of atoms added or removed). These different types of runs were applied iteratively until convergence seemed to be reached.

### III. RESULTS

#### A. Case studies

Before we present results whilst directly searching for the global minima in both composition and configuration space, it is useful to get a feel for the energetics as a function of composition. To do this, we map out the landscape associated with the energy of the global minima as a function of  $n_A$  and  $\sigma_{BB}/\sigma_{AA}$  for a number of examples, namely BLJ<sub>13</sub>, BLJ<sub>45</sub> and BLJ<sub>55</sub>. For the latter two, this represents a significant effort, since we have found the global minima at 1320 and 1620 different points in this space, respectively.

For BLJ<sub>13</sub>, the structure of the global minima is always the centred icosahedron, so Fig. 2(a) simply represents the variation of the energy of this one structure. Close to  $\sigma_{BB}/\sigma_{AA} = 1$ , as expected, the structure with one small atom at the centre of the cluster is the most stable composition. The distance between adjacent vertices of the perfect icosahedra is 5.15% longer than that between a vertex and the centre. Consistent with this, the strain energy goes to zero when  $\sigma_{BB}/\sigma_{AA}$  takes this value, i.e.  $\sigma_{BB}/\sigma_{AA} = 1.1085$ . The minimum in the total energy is displaced to slightly larger  $\sigma_{BB}/\sigma_{AA}$ , namely 1.1303, because this leads to a greater contribution to the energy from next neighbours. Beyond this, the energy of the AB<sub>12</sub> structure rises, and at  $\sigma_{BB}/\sigma_{AA} = 1.1614$ , the A<sub>4</sub>B<sub>9</sub> structure becomes the most stable composition. With three smaller atoms in the surface, this structure is more able to relieve the compressive strain that builds up in the AB<sub>12</sub> structure. With further increases in  $\sigma_{BB}/\sigma_{AA}$  the global minimum changes twice more with the number of A atoms increasing in order to achieve a lower strain energy. These transitions give a flat bottom to the landscape in Fig. 2(a).

BLJ<sub>45</sub> shows a much richer structural behaviour, because there are a variety of competing geometric structures. Firstly, there are two ways that atoms can be added around the 13-atom Mackay icosahedron, as illustrated in Fig. 3. In general, the Mackay overlayer continues the face-centred-cubic (fcc) packing of the twenty vertex-sharing fcc tetrahedra that make up a Mackay icosahedron, whereas the anti-Mackay overlayer adds atoms in sites that are hcp with respect to the fcc tetrahedra. The anti-Mackay layer has a lower surface density, and consequently has a greater number of nearest neighbours, but for monoatomic systems also a larger strain energy. Typically, therefore, growth starts off in the anti-Mackay overlayer, and then switches to the Mackay overlayer, as the layer grows.

For growth on the 13-atom icosahedron, the anti-Mackay overlayer maintains the polytetrahedral charac-

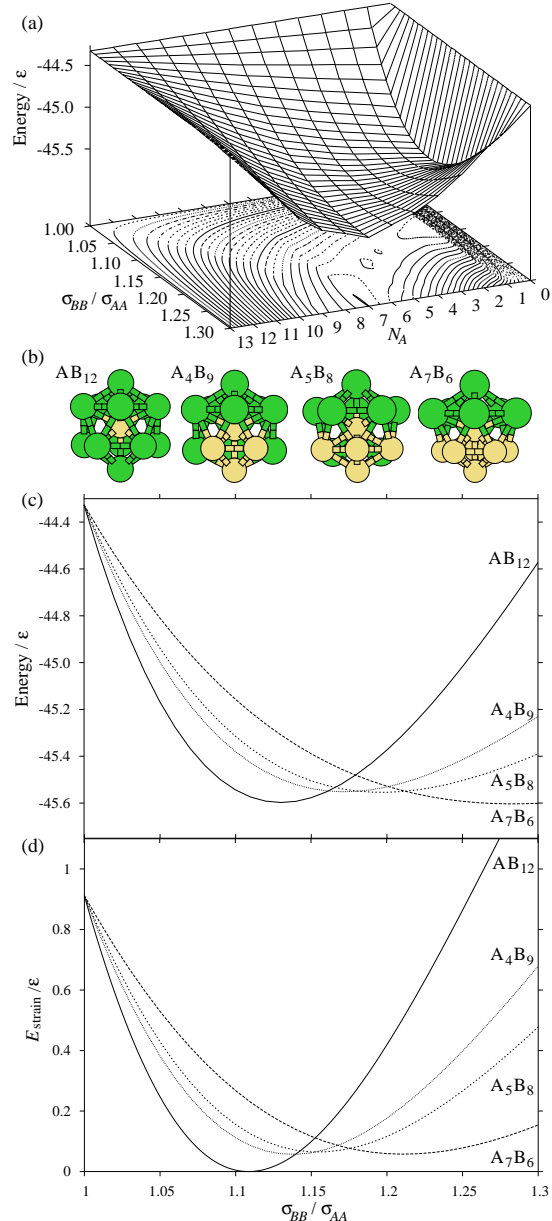


FIG. 2: (Colour online) BLJ<sub>13</sub>. (a) Landscape showing the dependence of the energy of the global minimum on  $\sigma_{BB}/\sigma_{AA}$  and  $n_A$ . (b) The four compositional global minima and the dependence of (c) their total energies and (c) strain energies on  $\sigma_{BB}/\sigma_{AA}$ .

ter of the structures with each interior atom having a local icosahedral coordination shell (we call such structures polyicosahedral), whereas the Mackay overlayer introduces some octahedral interstices into the structure. For LJ clusters,  $N = 31$  is the first size at which the global minimum adopts the Mackay overlayer.<sup>3</sup> We chose to examine BLJ<sub>45</sub> in detail, because at this size the anti-Mackay overlayer is able to be completed, giving a structure with point group  $I_h$  that we call the anti-Mackay

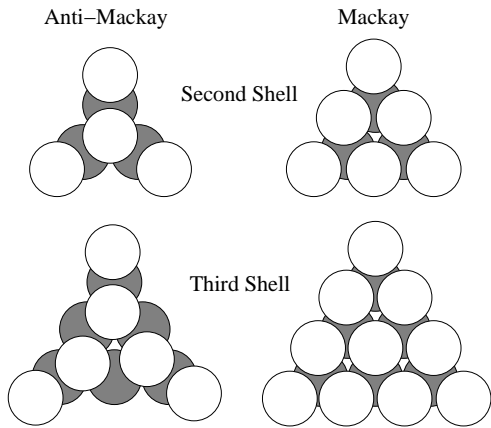


FIG. 3: The two possible overlayers for growth around a complete Mackay icosahedron. These are illustrated for a single face of the underlying 13-atom (top) and 55-atom (bottom) Mackay icosahedron.

icosahedron.

Secondly, there is the possibility of structures that are polytetrahedral, but that are not polyicosahedral. Instead, there are interior atoms that have a coordination number ( $Z$ ) greater than 12. For polyicosahedral structures, there are five tetrahedra around every interior edge. However, as we noted in the introduction, the corresponding packings of regular tetrahedra involve gaps that increase rapidly with the size of the packing (Fig. 1). As a consequence, it is not possible to generate a bulk polyicosahedral packing, and for clusters, the surface density decreases and the average nearest-neighbour distance between the surface atoms increases as the structures become bigger.

An alternative way to pack tetrahedra is to introduce some edges in the structure that have six tetrahedra around them. Such an arrangement is locally less favourable—for regular tetrahedra there is an overlap equivalent to  $63.17^\circ$ . However, for sufficiently large packings, the combination of ‘gaps’ and ‘overlaps’ allows one to generate structures that have less overall strain than polyicosahedral packings of the same size. For example, bulk polytetrahedral structures, called Frank-Kasper phases,<sup>21,22,23</sup> are now possible with these two types of edge environments. For clusters, such polytetrahedral structures have a higher surface density than polyicosahedral structures, and so need a smaller atomic size ratio to be stabilized in binary systems.

Those edges that have six tetrahedra around them are said to have disclination lines running along them, and such polytetrahedral structures can be viewed in terms of a network of disclination lines threading an icosahedrally-coordinated medium. Those atoms that have disclinations passing through them have a coordination number greater than 12. For example, 14-coordinate atoms have a single disclination line passing through them, and 15- and 16-coordinate atoms act as nodes for three and four disclination lines, respectively. We will

use the presence of these different types of Frank-Kasper coordination polyhedra to differentiate these polytetrahedral structures.

The  $(\sigma_{BB}/\sigma_{AA}, N_A)$  landscape associated with the  $BLJ_{45}$  global minimum is shown in Fig. 4. It is noteworthy that there is no optimal size ratio, but instead the energy of the global minimum decreases virtually monotonically with increasing size disparity. Also apparent is the magnitude of the stabilizations that can be achieved compared to monoatomic LJ clusters. The lowest-energy structure in the  $\sigma_{BB}/\sigma_{AA}$  range that we consider here is  $27.252\epsilon$  lower in energy than the  $LJ_{45}$  global minimum, i.e. a 12.7% decrease in the total energy.

There are four different compositional  $BLJ_{45}$  global minima in the parameter range studied. Near to  $\sigma_{BB}/\sigma_{AA} = 1$ , as one would expect the global minimum is icosahedral with a Mackay overlayer, and has the same geometric structure as for LJ clusters. The ideal composition of this structure depends slightly on  $\sigma_{BB}/\sigma_{AA}$ . At  $\sigma_{BB}/\sigma_{AA} = 1.057$  the polytetrahedral structure  $A_8B_{37}$  with a single negative disclination threading the structure becomes most stable. At  $\sigma_{BB}/\sigma_{AA} = 1.071$  the core-shell anti-Mackay icosahedron becomes most stable.

These changes are driven by a balance between the number of nearest neighbours and the strain energy of the structures. As  $\sigma_{BB}/\sigma_{AA}$  increases, structures with a larger number of nearest neighbours become the most stable, when their strain energy is sufficiently reduced. In this series, the number of nearest neighbours increases from 180 to 192 to 204, but at small  $\sigma_{BB}/\sigma_{AA}$  so does the strain energy also increase. In particular, notice that the strain energy for the polytetrahedral structure involving disclinations is less than the polyicosahedral structure (Fig. 4(b)).

These results illustrate how allowing two atoms of different sizes can substantially reduce the strain energy associated with polytetrahedral structures. For example, the strain energy of the anti-Mackay icosahedron can be decreased from  $24.4$  to  $1.7\epsilon$  (Fig 4e). However, unlike  $BLJ_{13}$ , the strain cannot be completely removed. There are only two different nearest-neighbour distances in a 13-atom icosahedron, whereas there are six different nearest-neighbour distances for the anti-Mackay icosahedron, and they cannot be adjusted so that they all have the same  $r_{ij}/\sigma_{\alpha\beta}$ .

When we also look at the compositional dependence of the global minimum in Fig. 4(b), we should remember that at  $N_A = 0$ ,  $N_A = N$  and  $\sigma_{BB}/\sigma_{AA} = 1$  the model is the same as the one-component Lennard-Jones model. Similarly, close to these values the structure has a Mackay overlayer, as for LJ clusters, i.e. for clusters with mostly A, mostly B or small  $\sigma_{BB}/\sigma_{AA}$ . By contrast, the polyicosahedral structures are most stable for intermediate compositions and larger  $\sigma_{BB}/\sigma_{AA}$ . For much of the structural phase diagram, sandwiched between these two structural types is a region where polytetrahedral structures with disclinations are most stable. However, there is some asymmetry, as at larger  $\sigma_{BB}/\sigma_{AA}$ , this zone is

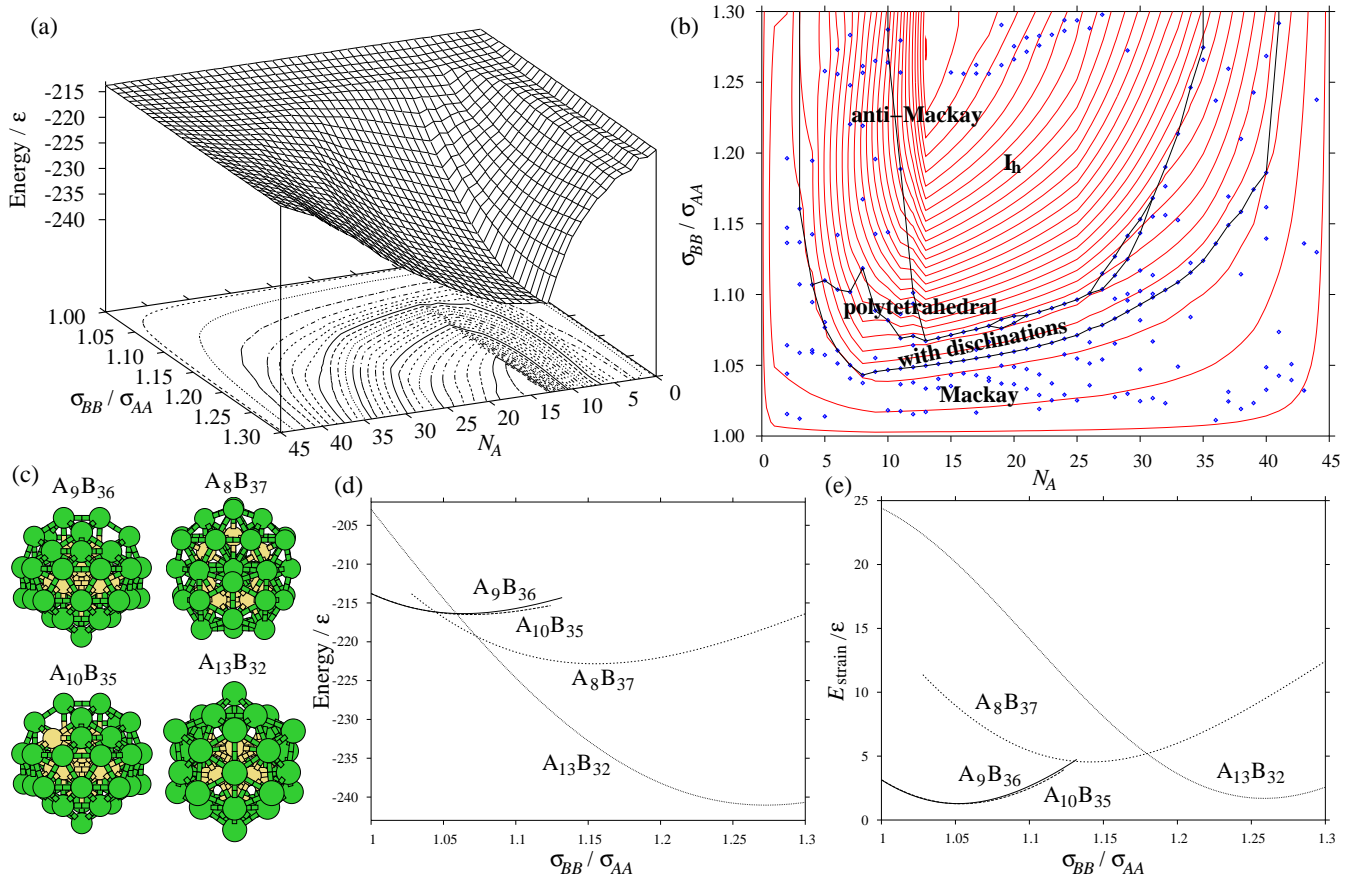


FIG. 4: (Colour online) BLJ<sub>45</sub>. (a) Landscape showing the dependence of the energy of the global minimum on  $\sigma_{BB}/\sigma_{AA}$  and  $N_A$ . (b) Zero-temperature structural phase diagram showing how the structure of the global minimum depends on  $\sigma_{BB}/\sigma_{AA}$  and  $N_A$ , superimposed on the contour plot of the landscape in (a). Each data point corresponds to a change in the structure of the global minimum as a function of  $\sigma_{BB}/\sigma_{AA}$ . The region where the anti-Mackay icosahedron is global minimum is labelled  $I_h$ . (c) The four compositional global minima and the dependence of (d) their total energies and (e) strain energies on  $\sigma_{BB}/\sigma_{AA}$ .

only found for larger values of  $N_A$ .

Our final case study is BLJ<sub>55</sub>. This size has been chosen, as it corresponds to the size at which a complete Mackay icosahedron is possible. Again, we illustrate the landscape associated with the global minimum and, in this case, the seven compositional global minima (Fig. 5). The overall behaviour is somewhat similar to BLJ<sub>45</sub>. There are four main differences. Firstly, the Mackay structures are most stable over a greater range of  $\sigma_{BB}/\sigma_{AA}$  and composition, which is unsurprising given that  $N = 55$  is a Mackay magic number. Secondly, there is a more pronounced change in slope in Fig. 5(a) associated with the onset of polytetrahedral structures. The landscape is relatively flat in the regions where Mackay structures are most favoured, but goes down more steeply, in the region where polytetrahedral structures are most stable, because the strain energy associated with these structures rapidly decreases, as the size disparity increases (Fig. 5(e)). Thirdly, polyicosahedral structures are most stable for a smaller range of parameters. This is because, as the size increase the

strain energy associated with these structures for the monoatomic LJ clusters increases rapidly, and hence the size difference that is needed to stabilize them also increases. Fourthly, as a corollary of the above, the area in Fig. 5(a) where polytetrahedral structures involving disclinations are more stable increases. Furthermore, there are two types of such structure, which can be differentiated by the nodes in the disclination network. The ‘Z14’ structures involve a single disclination line passing through the cluster, whereas the ‘Z15’ structures has three disclinations radiating out from the 15-coordinate atom.

For BLJ<sub>55</sub>, the compositional global minimum changes six times as  $\sigma_{BB}/\sigma_{AA}$  increases. First, there is the core-shell Mackay icosahedron. Although the strain in this structure is much less than for polytetrahedral structures, the strain energy can still be significantly reduced compared to the LJ case by introduction of different-sized atoms (Fig. 5(e)). For example, this structure has its lowest energy at  $\sigma_{BB}/\sigma_{AA} = 1.064$ . The next three compositional global minimum are polytetrahedral structures

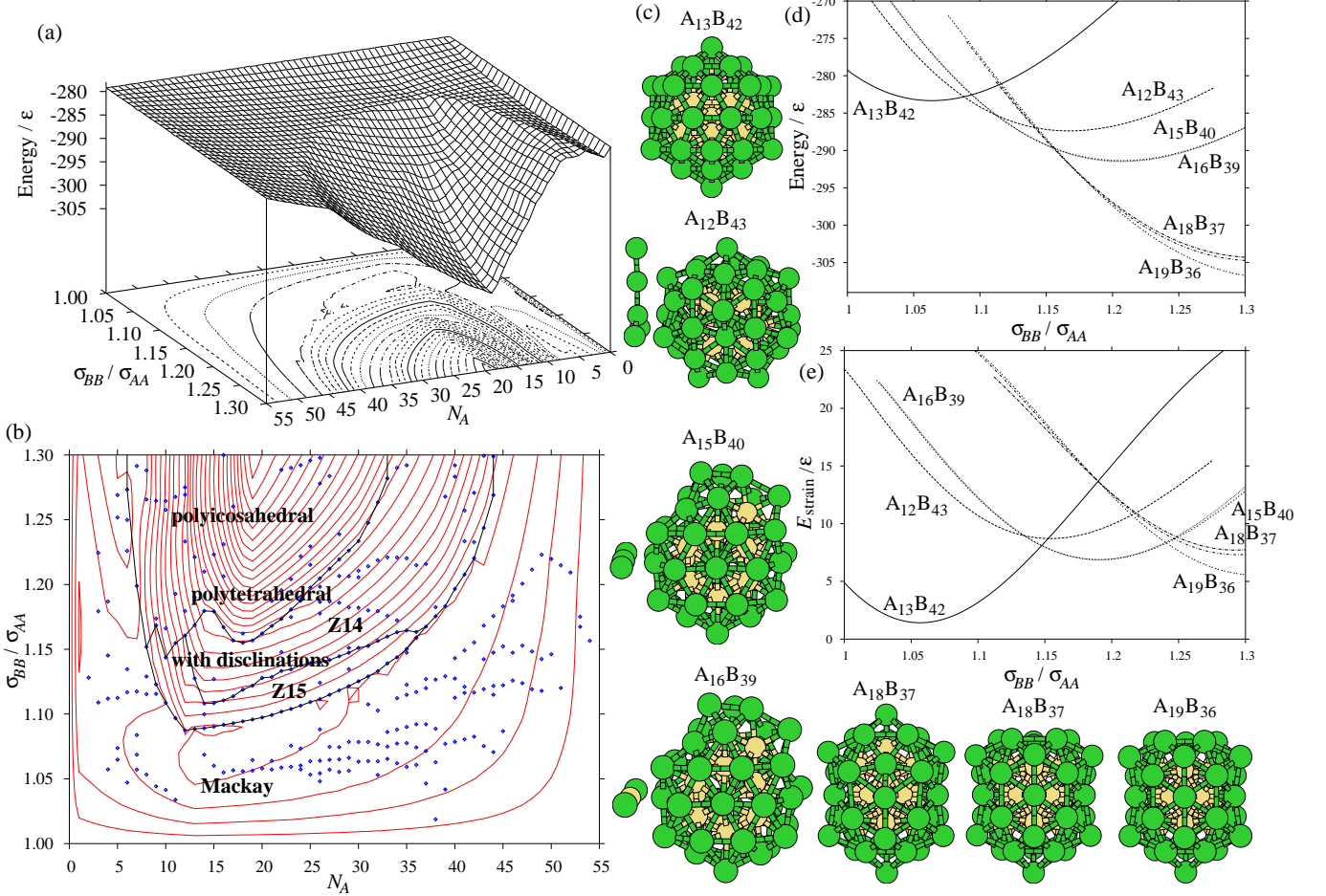


FIG. 5: (Colour online) BLJ<sub>55</sub>. (a) Landscape showing the dependence of the energy of the global minimum on  $\sigma_{BB}/\sigma_{AA}$  and  $N_A$ . (b) Zero-temperature structural phase diagram showing how the structure of the global minimum depends on  $\sigma_{BB}/\sigma_{AA}$  and  $N_A$ , superimposed on the contour plot of the landscape in (a). Each data point corresponds to a change in the structure of the global minimum as a function of  $\sigma_{BB}/\sigma_{AA}$ . The region where polytetrahedral structures involving disclinations are the global minima is divided into two subregions, depending on whether the highest coordination number for an atom is 14 or 15. (c) The seven compositional global minima and the dependence of (d) their total energies and (e) strain energies on  $\sigma_{BB}/\sigma_{AA}$ . In (c) for the relevant global minima the disclination networks are depicted to the left of the structure.

that involve disclination lines. Note, that the Z15 structure is more stable at smaller  $\sigma_{BB}/\sigma_{AA}$  as it involves a greater disclination density than the Z14 structures. These structures are not pure core-shell clusters, as although all the 12-coordinate interior atoms are A atoms, there is a preference for the larger atoms to lie on the disclinations, which is unsurprising given their higher coordination number. The final three compositional global minima are polyicosahedral, and differ just in the position of capping atoms and composition.

## B. Compositional global minima

In this section, we focus our attention on the compositional global minima. Figs. 6, 7, 8, and 9, summarize the results. The energies and points files for all the pu-

tative global minima are available online.<sup>44</sup> In Fig. 6, the energies at different size ratio are compared. This figure clearly illustrates that, as noted in the above case studies, the energy virtually monotonically decreases with increasing size ratio. It also shows the substantial nature of the stabilizations that are achieved compared to the one-component Lennard-Jones system.

In Fig. 7, the energies at the six size ratios we consider are plotted in a way that reveals the particularly stable sizes. In Fig. 8 we show some of the particularly interesting or stable structures associated with the different structural types.

Fig. 9 provides a structural phase diagram showing how the  $(N, \sigma_{BB}/\sigma_{AA})$  plane can be divided into regions where the compositional global minima have the same type of structure. To construct this diagram, we considered intervals of 0.01 in  $\sigma_{BB}/\sigma_{AA}$  and reoptimized the

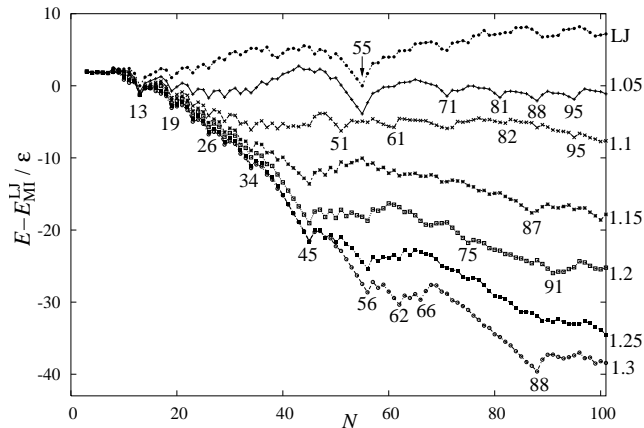


FIG. 6: The energy of the BLJ global minimum for the six values of  $\sigma_{BB}/\sigma_{AA}$  studied, relative to  $E_{ML}^{LJ}$ , a fit to the energies of the Mackay icosahedra for LJ clusters. A line corresponding to the LJ global minima is also included

five lowest-energy structures from the nearest size ratios for which global optimization was performed. Then, we checked if the structure of the global minimum changes in any of these intervals, and if so we obtained the precise value of  $\sigma_{BB}/\sigma_{AA}$  at which this change took place. Of course, this approach will potentially miss the true global minima at intermediate values of  $\sigma_{BB}/\sigma_{AA}$  if it is not one of the five best for the values at which we ran the global optimization algorithm, and it only allows for one change in the global minimum in any 0.01 interval. However, we are concerned more with the overall form of this diagram, on which these approximations will only have a very minor effect.

The reference system to which to compare our results is, of course, the one-component LJ clusters, for which structures based on the Mackay icosahedra are dominant in the current size range. Growth around the 13-atom icosahedron initially occurs in the anti-Mackay overlayer, but for  $LJ_{31}$  and beyond the global minimum has a Mackay overlayer.<sup>3</sup> Similarly, for the growth of the next icosahedral shell, the global minima initially have an anti-Mackay overlayer, but for  $LJ_{82}$  and beyond (with the exception of  $LJ_{85}$ ) the Mackay overlayer is more stable. The only exceptions to this dominance of icosahedral structures are for  $LJ_{38}$ ,  $LJ_{75-77}$  and  $LJ_{98}$  for which an fcc truncated octahedron, Marks decahedra<sup>45</sup> and a Leary tetrahedron,<sup>46</sup> respectively, are just more stable than the competing icosahedral structures.

As one moves away from  $\sigma_{BB}/\sigma_{AA} = 1$  in the structural phase diagram, firstly icosahedral structures quickly become more stable than the five non-icosahedral structures mentioned above. Secondly, for both the second and third icosahedral shells the crossover size at which the Mackay overlayer becomes more stable is pushed to larger sizes (Fig. 9). This is because the anti-Mackay overlayer is more strained, and so the introduction of two atomic sizes can lead to a greater reduction in its strain

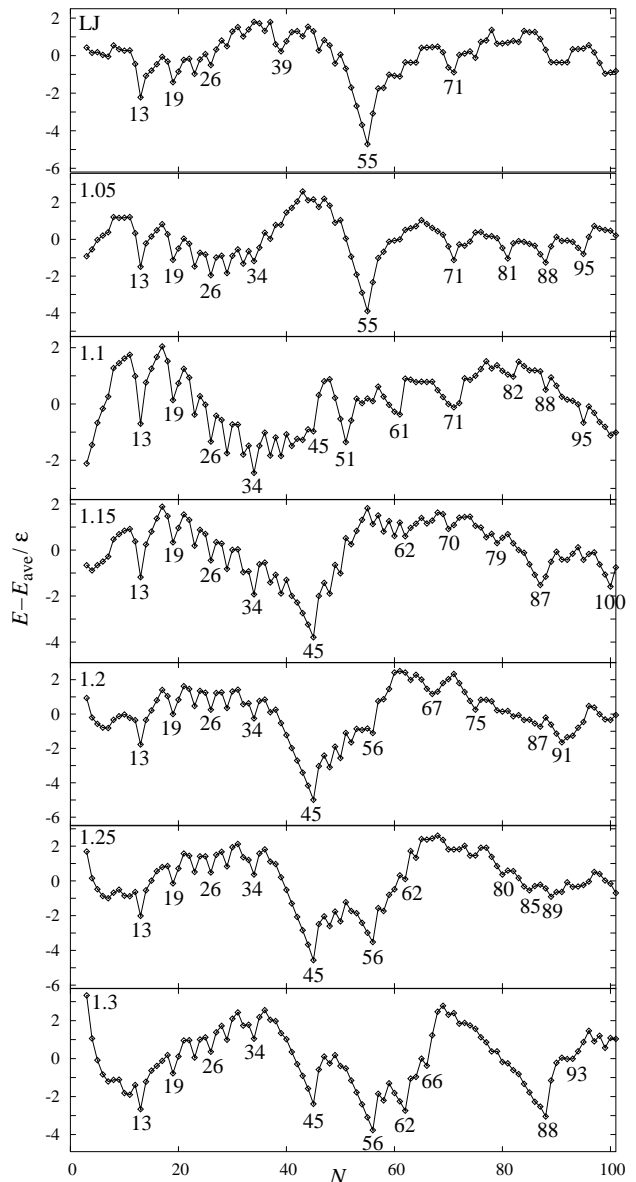


FIG. 7: The seven panels correspond to the energies of the global minimum for the six values of  $\sigma_{BB}/\sigma_{AA}$  studied and for the one-component LJ clusters, relative to  $E_{ave}(\sigma_{BB}/\sigma_{AA})$ , a fit to the energies of the global minima at that size ratio using the form  $a + bN^{1/3} + cN^{2/3} + dN$ .

energy. For both types of overlayer, the larger atoms will preferentially go into the surface layer, because of the tensile strain in the surface of the icosahedral LJ clusters, leading to the formation of core-shell clusters, as already illustrated by  $A_{13}B_{32}$  and  $A_{13}B_{42}$  in the previous section. There are many further examples in Fig. 8. As for the 13-atom icosahedron considered in the last section, there is an optimal size ratio for these core-shell structures. Beyond this, compressive strains begin to build up in the surface until at some point it becomes favourable to include some of the smaller A atoms in the surface.

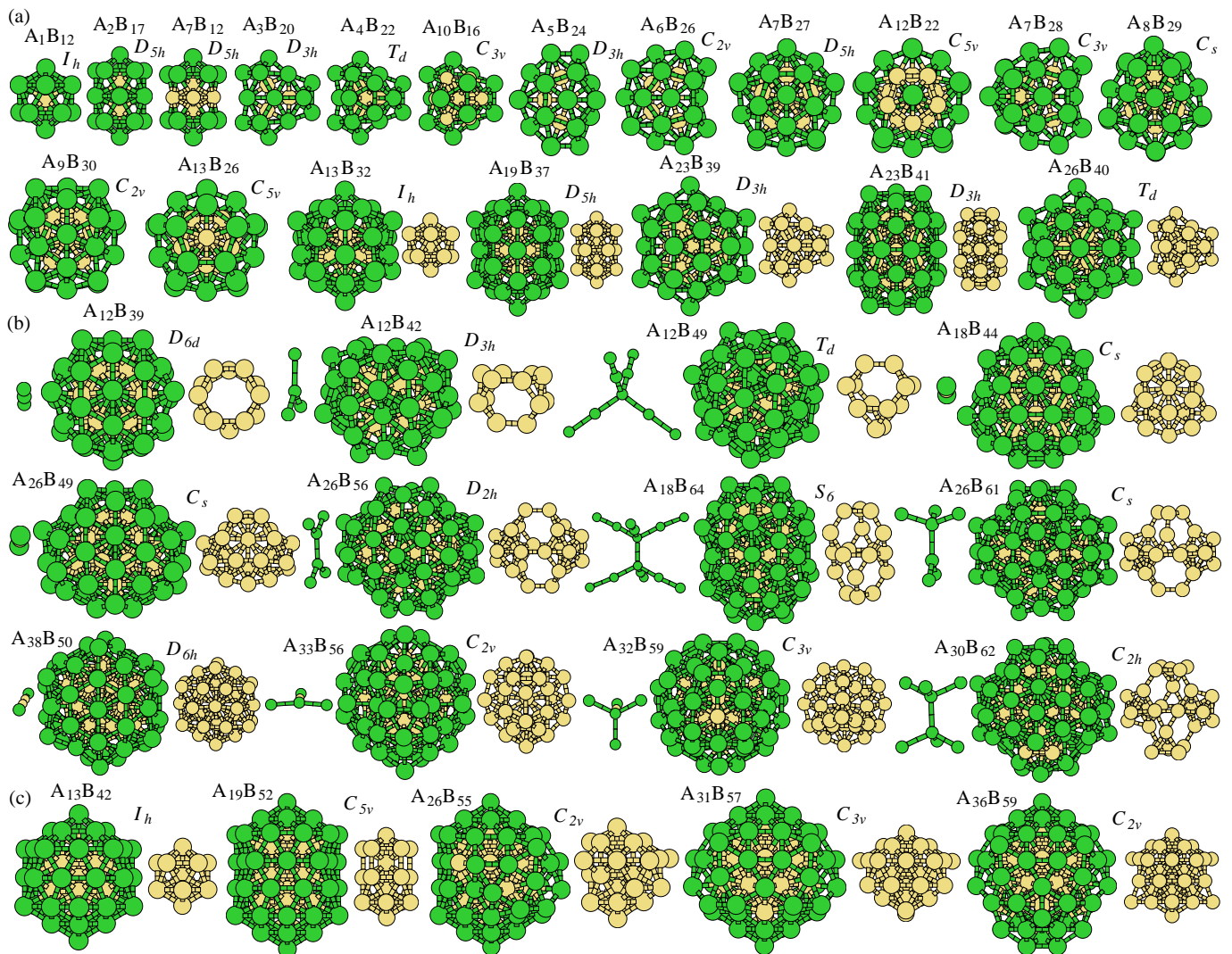


FIG. 8: (Colour online) A selection of the particularly stable BLJ global minima grouped according to their structural type: (a) polycosahedral, (b) polytetrahedral with disclinations and (c) the 55-atom Mackay icosahedron with an anti-Mackay overlayer. For the larger clusters, to the right of the cluster, the A-atom core is also depicted, and in (b) to the left is the disclination network.

Some examples of the structures that result are shown in Fig. 8(a), e.g.  $A_7B_{12}$ ,  $A_{10}B_{16}$  and  $A_{12}B_{22}$ . However, the window of  $\sigma_{BB}/\sigma_{AA}$  values for which these core-shell structures are most stable is wide, illustrating their particular stability.

This preference for the anti-Mackay overlayer can also be seen in the observed magic numbers (Fig. 7). For the second shell, anti-Mackay clusters are particularly stable at  $N=19$ , 23, 26 and 29 for LJ clusters, and correspond to 2, 3, 4 and 5 interpenetrating icosahedra. These become more prominent as  $\sigma_{BB}/\sigma_{AA}$  increases with additional magic numbers at  $N=34$  and 45, and to a lesser extent at  $N=32$ , 37 and 39. The magic number at  $N = 45$  is particularly strong as it corresponds to the completion of the anti-Mackay overlayer. Interestingly, beyond  $N = 34$  the way the anti-Mackay overlayer grows depends on  $\sigma_{BB}/\sigma_{AA}$ . At smaller  $\sigma_{BB}/\sigma_{AA}$  the formation

of structures that can be thought of as interpenetrating complete icosahedra continues, as illustrated by  $A_9B_{30}$ . In contrast, at larger  $\sigma_{BB}/\sigma_{AA}$  the sites above the faces of the central 13-atom icosahedra are completely filled and further growth occurs just by adding atoms above the vertices (Fig. 3), e.g.  $A_{13}B_{26}$ .

Similarly, for the third shell, as well as the magic number at  $N=71$  already present for LJ clusters, additional magic numbers appear at 81, 88 and 95. These correspond to covering five, eight, ten and twelve faces of the underlying Mackay icosahedron, respectively.

As already mentioned, clusters with an anti-Mackay overlayer covering the 13-atom icosahedron are polycosahedral in character. However, there is no reason why this type of packing should not continue beyond the completion of this overlayer at  $N = 45$ . Indeed, for the range of  $\sigma_{BB}/\sigma_{AA}$  values considered here such structures are pos-

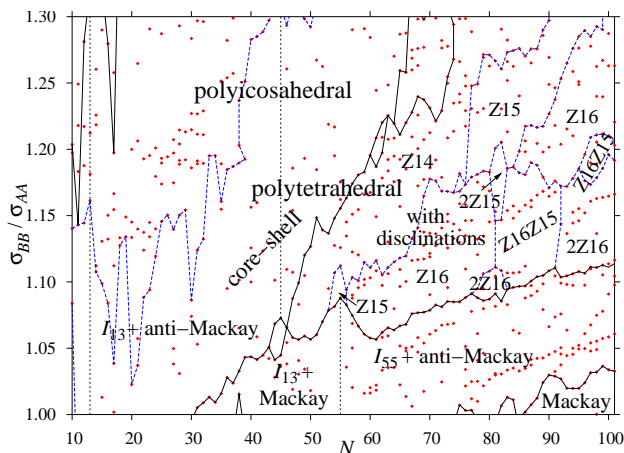


FIG. 9: (Colour online) Structural phase diagram showing how the structure of the global minimum depends on  $N$  and  $\sigma_{BB}/\sigma_{AA}$ . Each point corresponds to the value of  $\sigma_{BB}/\sigma_{AA}$  at which the global minimum for a given  $N$  changes. The lines divide the diagram into regions where the global minima have the same structural type. The labels  $I_{13}$  and  $I_{55}$  stand for the 13- and 55-atom Mackay icosahedra.

sible up until  $N = 69$ , and the magic numbers at  $N=56$ , 62 and 66 that appear at larger  $\sigma_{BB}/\sigma_{AA}$  correspond to core-shell polyicosahedral structures with the double, triple and quadruple icosahedra as their core (Fig. 8(a)). Also interesting is the  $A_{23}B_{41}$  structure, for which the core of A atoms is two face-sharing icosahedra.

In the structural phase diagram as  $N$  increases a region opens up between the Mackay icosahedral and polyicosahedral structures, where polytetrahedral structures involving disclinations are most stable. The first such structure occurs at  $N = 44$  and as  $N$  increases, these structures occupying an increasing proportion of the phase diagram. These structures are not seen at small size, firstly because the strain associated with polyicosahedral structures is not prohibitively high, and secondly because the introduction of disclinations would lead to high disclination densities, and unfavourable strain energies. For this reason the Frank-Kasper coordination polyhedra that are possible at  $N=15, 16$  and  $17$  are never most stable.

Later when substantial strains have built up in the polyicosahedral structures, the introduction of disclinations along a small minority of the edges can lead to a reduction in the overall strain energy. The structures  $A_{12}B_{39}$ ,  $A_{12}B_{42}$  and  $A_{12}B_{49}$  provide interesting examples, and correspond to the covering of the above Frank-Kasper coordination polyhedra by a complete anti-Mackay-like overlayer with atoms added above every face and vertex (except the six-fold vertices for the 51- and 54-atom structures).

At larger sizes more complex disclination networks are possible. For example the  $2Z16$  structures, e.g.  $A_{18}B_{64}$ ,  $A_{30}B_{62}$ , have two nodes where four disclinations meet, and gives rise to an ethane-like disclination network, and

the  $Z15Z16$  structures, e.g.  $A_{26}B_{61}$ , have one node where three disclinations meet, and one where four meet.

From Fig. 9 some systematic trends in the character of the disclination networks are clear. As  $N$  increases, the structures next to the Mackay icosahedral-polytetrahedral boundary have an increasing number of disclinations in order to reduce the growing strains that would have otherwise occurred. However, as  $\sigma_{BB}/\sigma_{AA}$  increases the different-sized atoms are able to reduce some of this strain, and the disclination density goes down, until the boundary with disclination-free polyicosahedral structures is reached. So, for example, for  $BLJ_{82}$  the structure changes from  $2Z16$ , to  $Z16Z15$  to  $Z15$  to  $Z14$  as  $\sigma_{BB}/\sigma_{AA}$  increases.

#### IV. CONCLUSIONS

In this paper we have introduced a new global optimization approach for binary clusters that for a given size searches directly for the composition of greatest stability. This development makes it tractable to explore the size evolution of binary cluster structure systematically, rather than just arbitrarily selecting particular sizes or compositions. Of course, by focussing on the compositional global minimum, some information is lost, but as one is usually most interested in identifying the most stable magic number clusters, this is of little import. Besides the alternative approach of finding the global minimum at each size and composition would both be computationally extremely challenging and result in a surfeit of information, the added value of which is far from clear. The approach is straightforward to apply to other binary systems, and, for example, we have just completed applying this approach to all clusters with up to 150 atom for a number of binary metal systems.<sup>47</sup>

One of the most important aims of theoretical studies of structure is to provide models that can aid the interpretation of experimental observations. In this regard, it is reasonable to ask whether our approach of optimizing the composition is realistic of what might be occurring experimentally. The answer would of course depend on how the binary clusters are produced experimentally, but recent experiments on copper-tin clusters showed that the particularly stable compositions could be obtained after annealing the clusters.<sup>48</sup>

We have used the current approach to systematically explore the structural effects of having different-sized atoms on binary LJ clusters. Particularly interesting is how this stabilizes polytetrahedral clusters, both those that are polyicosahedral and those that involve disclinations, which for the one-component LJ clusters are too strained to be competitive. The effects of the two atom sizes is somewhat similar to other methods of strain relief, such as widening the potential well, which also pushes the anti-Mackay to Mackay transitions to larger size and stabilizes polytetrahedral structures with disclination lines.<sup>45,49</sup> In future work, we plan to extend our

exploration of the BLJ system to other choices for the four parameters in the potential, and to help develop its status as an archetypal model system for which to understand the structure of binary clusters.

Our results have provided a zoo of interesting structures, which are good candidates for particularly stable clusters for binary systems where the two atom types have significant differences in size. Although BLJ clusters are not a realistic model for much, except for rare gas mixtures at certain parameter choices, as for monoatomic LJ clusters, our expectation is that the stable structural forms seen for the BLJ clusters are robust, and likely to be relevant for a wide variety of systems, where the interactions are approximately isotropic. This confidence is based on previous experience, where particular structural forms first seen for a model system are later found in real systems. For example, the Leary tetrahedron,<sup>46</sup> which was first discovered as the global minimum for LJ<sub>98</sub>, was later found to be one of the dominant structural forms for clusters of C<sub>60</sub> molecules.<sup>50</sup> Indeed, core-shell polyicosahedral structures have already been found for binary metal clusters, such as the Ag-Ni and Ag-Cu systems.<sup>14,15,47,51</sup>

In this paper, we have focussed on the global minima of our system, and so Fig. 9 represents the structural phase diagram at zero temperature. It is, therefore legitimate to ask how our results would be affected by temperature. Firstly, for sufficiently small size differences between the atoms, it is likely that there will be low-temperature order-disorder transitions, where the geometric structure is retained, but the permutational order is lost.<sup>33,43</sup> However, as  $\sigma_{BB}/\sigma_{AA}$  increases, these transitions are likely to become less common, because the A and B atoms quickly develop strongly preferred positions, as, for example, in the core-shell ordering.

Secondly, it is known for the LJ system that an effect of temperature is to push the anti-Mackay to Mackay transition to larger size,<sup>52,53,54,55</sup> because of the greater vibrational entropy of the anti-Mackay structures.<sup>11</sup> Indeed, the form of Fig. 9 at small  $\sigma_{BB}/\sigma_{AA}$  looks similar to the  $(N, T)$  structural phase diagram for LJ clusters.<sup>53,54</sup> Therefore, temperature will reinforce the stabilization of polytetrahedral structures seen for BLJ clusters.

Here, we have probed all BLJ clusters with up to 100 atoms. But what would one expect at larger sizes, and in the bulk limit? The dominance of polytetrahedral structures in the current size range is because of their favourable surface energetics, and it can be seen in Fig. 9 that the range of stability for non-polytetrahedral clusters is increasing as  $N$  increases. The latter would suggest that Frank-Kasper phases are never the ground state in the bulk limit. Instead, phase-separated A and B fcc crystals are likely to have the lowest energy for bulk.

However, one cannot rule out that this boundary might flatten off at larger sizes, nor that there might be some range of temperature and pressure, where Frank-Kasper phases might be most stable.

The reverse of the above prediction is that there are likely to be binary systems, which although they do not have any stable bulk Frank-Kasper phases, nevertheless exhibit Frank-Kasper-like structures for their clusters. Indeed, we have already identified such structures for Ni-Al, Ag-Cu and Ag-Ni clusters using the current methodology.<sup>47</sup> Although likely to be less common than for binary clusters, there are a few one-component systems that also exhibit these polytetrahedral clusters.<sup>49,56,57</sup>

Our results are also of relevance for understanding the effect of size mismatch on glass formation. In order to explain the difficulty of homogeneous nucleation in supercooled metal droplets, Frank argued that if the preferred local order within the liquid was incompatible with the local structure in the crystal, nucleation would be suppressed because of the substantial structural rearrangement required.<sup>58</sup> Furthermore, he used the structures of isolated LJ clusters, in particular the stability of the 13-atom icosahedron compared to an fcc cluster of the same size, to provide a picture of the local order within the liquid. More recently, the predictive power of isolated clusters for understanding liquid structure has received significant empirical support.<sup>59,60,61</sup>

Empirically, it has been found that one of the conditions for metallic alloys to form bulk glasses is that there is a size difference of at least 12%.<sup>62</sup> A simple theoretical justification of this can be given in terms of the size difference required to destabilize a crystalline solid solution.<sup>63,64</sup> For the current system, the critical value of  $\sigma_{BB}/\sigma_{AA}$  at which a solid solution is no longer always stable has been found to be 1.20.<sup>65</sup> Although the determinants of glass-forming ability are subtle,<sup>66,67</sup> and more sophisticated theories can be developed,<sup>68,69,70</sup> our results highlight the potential role played by the local structure within the liquid,<sup>71</sup> and how size differences can stabilize local polytetrahedral, in particular icosahedral,<sup>72</sup> order, and hence frustrate crystallization. Indeed, one of the commonly used model glass-forming systems used in the simulation community is a 50:50 BLJ mixture with  $\sigma_{BB}/\sigma_{AA} = 1.2$ , and all other parameters as in the present study.<sup>73,74,75</sup>

## Acknowledgments

J.P.K.D is grateful to the Royal Society for financial support.

---

<sup>1</sup> A. F. Lee, C. J. Baddeley, C. Hardacre, R. M. Ormerod, R. M. Lambert, G. Schmid, and W. Heike, *J. Phys. Chem.*

- <sup>2</sup> A. M. Molenbroek, S. Haukka, and B. S. Clausen, *J. Phys. Chem. B* **102**, 10680 (1998).
- <sup>3</sup> J. A. Northby, *J. Chem. Phys.* **87**, 6166 (1987).
- <sup>4</sup> D. J. Wales and J. P. K. Doye, *J. Phys. Chem. A* **101**, 5111 (1997).
- <sup>5</sup> D. Romero, C. Barrón, and S. Gómez, *Comput. Phys. Commun.* **123**, 87 (1999).
- <sup>6</sup> Y. Xiang, H. Jiang, W. Cai, and X. Shao, *J. Phys. Chem. A* **108**, 3586 (2004).
- <sup>7</sup> Y. Xiang, L. Cheng, W. Cai, and X. Shao, *J. Phys. Chem. A* **108**, 9516 (2004).
- <sup>8</sup> X. Shao, Y. Xiang, and W. Cai, *J. Phys. Chem. A* **109**, 5193 (2005).
- <sup>9</sup> B. Raoult, J. Farges, M.-F. de Feraudy, and G. Torchet, *Philos. Mag. B* **60**, 881 (1989).
- <sup>10</sup> J. P. K. Doye and F. Calvo, *Phys. Rev. Lett.* **86**, 3570 (2001).
- <sup>11</sup> J. P. K. Doye and F. Calvo, *J. Chem. Phys.* **116**, 8307 (2002).
- <sup>12</sup> J. Jellinek and E. B. Krissinel, *Chem. Phys. Lett.* **258**, 283 (1996).
- <sup>13</sup> G. Rossi, R. Ferrando, A. Rapallo, A. Fortunelli, B. C. Curley, L. D. Lloyd, and R. L. Johnston, *J. Chem. Phys.* **122**, 194309 (2005).
- <sup>14</sup> G. Rossi, A. Rapallo, C. Mottet, A. Fortunelli, F. Baletto, and R. Ferrando, *Phys. Rev. Lett.* **93**, 105503 (2004).
- <sup>15</sup> A. Rapallo, G. Rossi, R. Ferrando, A. Fortunelli, B. C. Curley, L. D. Lloyd, G. M. Tarbuck, and R. L. Johnston, *J. Chem. Phys.* **122**, 194308 (2005).
- <sup>16</sup> F. Calvo and E. Yurtsever, *Phys. Rev. B* **70**, 045423 (2004).
- <sup>17</sup> C. Rey, J. García-Rodeja, and L. J. Gallego, *Phys. Rev. B* **54**, 2942 (1996).
- <sup>18</sup> C. Massen, T. V. Mortimer-Jones, and R. L. Johnston, *J. Chem. Soc., Dalton Trans.* pp. 4375–4388 (2002).
- <sup>19</sup> M. S. Bailey, N. T. Wilson, C. Roberts, and R. L. Johnston, *Eur. Phys. J. D* **25**, 41 (2003).
- <sup>20</sup> D. R. Nelson and F. Spaepen, *Solid State Phys.* **42**, 1 (1989).
- <sup>21</sup> D. P. Shoemaker and C. B. Shoemaker, in *Introduction to Quasicrystals*, edited by M. V. Jaric (Academic Press, London, 1988), pp. 1–57.
- <sup>22</sup> F. C. Frank and J. S. Kasper, *Acta Crystallogr.* **11**, 184 (1958).
- <sup>23</sup> F. C. Frank and J. S. Kasper, *Acta Crystallogr.* **12**, 483 (1959).
- <sup>24</sup> J. P. K. Doye and L. Meyer, *Phys. Rev. Lett.* **95**, 063401 (2005).
- <sup>25</sup> I. L. Garzón, X. P. Long, R. Kawai, and J. H. Weare, *Chem. Phys. Lett.* **158**, 525 (1989).
- <sup>26</sup> A. S. Clarke, R. Kapral, B. Moore, G. N. Patey, and X.-G. Wu, *Phys. Rev. Lett.* **70**, 3283 (1993).
- <sup>27</sup> A. S. Clarke, R. Kapral, and G. N. Patey, *J. Chem. Phys.* **101**, 2432 (1994).
- <sup>28</sup> C. Rey and L. J. Gallego, *Phys. Rev. B* **51**, 13691 (1995).
- <sup>29</sup> S. Cozzini and M. Ronchetti, *Phys. Rev. B* **53**, 12040 (1996).
- <sup>30</sup> D. H. Robertson, F. B. Brown, and I. M. Navon, *J. Chem. Phys.* **90**, 3221 (1989).
- <sup>31</sup> L. J. Munro, A. Tharrington, and K. D. Jordan, *Comput. Phys. Commun.* **145**, 1 (2002).
- <sup>32</sup> S. M. Cleary and H. R. Mayne, *Chem. Phys. Lett.* **418**, 79 (2006).
- <sup>33</sup> D. D. Frantz, *J. Chem. Phys.* **107**, 1992 (1997).
- <sup>34</sup> D. Sabo, J. D. Doll, and D. L. Freeman, *J. Chem. Phys.* **118**, 7321 (2003).
- <sup>35</sup> D. Sabo, J. D. Doll, and D. L. Freeman, *J. Chem. Phys.* **121**, 847 (2004).
- <sup>36</sup> D. Sabo, C. Predescu, J. D. Doll, and D. L. Freeman, *J. Chem. Phys.* **121**, 856 (2004).
- <sup>37</sup> Previously, we have defined the strain energy with respect to the equilibrium pair separation,<sup>45</sup> rather than the average nearest-neighbour distance. The problem with this previous definition is that essentially unstrained structures normally have an average neighbour distance that is smaller than the equilibrium pair separation, because this decreases  $E_{\text{nnn}}$  at the expense of a smaller increase in  $E_{\text{nn}}$ .
- <sup>38</sup> Z. Li and H. A. Scheraga, *Proc. Natl. Acad. Sci. USA* **84**, 6611 (1987).
- <sup>39</sup> J. P. K. Doye and D. J. Wales, *Phys. Rev. Lett.* **80**, 1357 (1998).
- <sup>40</sup> J. P. K. Doye, D. J. Wales, and M. A. Miller, *J. Chem. Phys.* **109**, 8143 (1998).
- <sup>41</sup> C. J. Tsai and K. D. Jordan, *J. Phys. Chem.* **97**, 11227 (1993).
- <sup>42</sup> F. H. Stillinger, *Phys. Rev. E* **59**, 48 (1999).
- <sup>43</sup> G. E. Lopez and D. L. Freeman, *J. Chem. Phys.* **98**, 1428 (1993).
- <sup>44</sup> The Cambridge Cluster Database, <http://www-wales.ch.cam.ac.uk/CCD.html>.
- <sup>45</sup> J. P. K. Doye, D. J. Wales, and R. S. Berry, *J. Chem. Phys.* **103**, 4234 (1995).
- <sup>46</sup> R. H. Leary and J. P. K. Doye, *Phys. Rev. E* **60**, R6320 (1999).
- <sup>47</sup> J. P. K. Doye and R. Ferrando, in preparation.
- <sup>48</sup> G. A. Breaux, D. A. Hillman, C. M. Neal, and M. F. Jarrold, *J. Phys. Chem. A* **109**, 8755 (2005).
- <sup>49</sup> J. P. K. Doye and D. J. Wales, *J. Chem. Soc., Faraday Trans.* **93**, 4233 (1997).
- <sup>50</sup> W. Branz, N. Malinowski, H. Schaber, and T. P. Martin, *Chem. Phys. Lett.* **328**, 245 (2000).
- <sup>51</sup> R. Ferrando, A. Fortunelli, and G. Rossi, *Phys. Rev. B* **72**, 085449 (2005).
- <sup>52</sup> F. Calvo and J. P. K. Doye, *Phys. Rev. E* **63**, 010902(R) (2001).
- <sup>53</sup> P. A. Frantsuzov and V. A. Mandelshtam, *Phys. Rev. E* **72**, 037102 (2005).
- <sup>54</sup> D. D. Frantz, *J. Chem. Phys.* **115**, 6136 (2001).
- <sup>55</sup> E. G. Noya and J. P. K. Doye, *J. Chem. Phys.* **124**, 104503 (2006).
- <sup>56</sup> J. P. K. Doye and D. J. Wales, *Phys. Rev. Lett.* **86**, 5719 (2001).
- <sup>57</sup> J. P. K. Doye, *J. Chem. Phys.* **119**, 1136 (2003).
- <sup>58</sup> F. C. Frank, *Proc. R. Soc. London, Ser. A* **215**, 43 (1952).
- <sup>59</sup> J. P. K. Doye, D. J. Wales, and S. I. Simdyankin, *Faraday Discuss.* **118**, 159 (2001).
- <sup>60</sup> M. Dzugutov, S. I. Simdyankin, and F. H. M. Zetterling, *Phys. Rev. Lett.* **89**, 195701 (2002).
- <sup>61</sup> J. P. K. Doye, D. J. Wales, F. H. Zetterling, and M. Dzugutov, *J. Chem. Phys.* **118**, 2792 (2003).
- <sup>62</sup> A. Inoue, *Acta Mater.* **48**, 279 (2000).
- <sup>63</sup> T. Egami and Y. Waseda, *J. Non-Cryst. Solids* **64**, 113 (1984).
- <sup>64</sup> T. Egami, *Mater. Sci. Eng. A* **226-228**, 261 (1997).
- <sup>65</sup> M. Li and W. L. Johnson, *Phys. Rev. Lett.* **70**, 1120 (1993).
- <sup>66</sup> J. R. Fernández and P. Harrowell, *J. Chem. Phys.* **120**, 9222 (2004).
- <sup>67</sup> P. Jalali and M. Li, *Phys. Rev. B* **71**, 014206 (2005).

- <sup>68</sup> O. N. Senkov and D. B. Miracle, *Mater. Res. Bull.* **36**, 2183 (2001).
- <sup>69</sup> D. B. Miracle, W. B. Sanders, and O. N. Senkov, *Philos. Mag.* **83**, 2409 (2003).
- <sup>70</sup> O. N. Senkov, D. B. Miracle, and H. M. Mullens, *J. Appl. Phys.* **97**, 103502 (2005).
- <sup>71</sup> J. R. Fernández and P. Harrowell, *J. Phys. Chem. B* **108**, 6850 (2004).
- <sup>72</sup> J. Lee, I.-H. Lee, and J. Lee, *Phys. Rev. Lett.* **91**, 080201 (2003).
- <sup>73</sup> G. Wahnström, *Phys. Rev. A* **44**, 3572 (1991).
- <sup>74</sup> T. B. Schrøder, S. Sastry, J. C. Dyre, and S. C. Glotzer, *J. Chem. Phys.* **112**, 9834 (2000).
- <sup>75</sup> N. Lačević, F. W. Starr, T. B. Schrøder, and S. C. Glotzer, *J. Chem. Phys.* **119**, 7372 (2003).